analytical chemistry

Technical Note

Cite This: Anal. Chem. XXXX, XXX, XXX−XXX

pubs.acs.org/ac

Assembled Step Emulsification Device for Multiplex Droplet Digital Polymerase Chain Reaction

Mengyue Nie,[†,#] Meng Zheng,[†,⊗] Caiming Li,[†,#] Feng Shen,[§] Manhua Liu,[∥] Haibei Luo,[⊥] Xiaohui Song,[⊥] Ying Lan,[*,†] Jian-Zhang Pan,[*,‡] and Wenbin Du[*,†,#,⊗]

[†]State Key Laboratory of Microbial Resources, Institute of Microbiology, Chinese Academy of Sciences, 100101, Beijing, China

[‡]Institute of Microanalytical Systems, Department of Chemistry, Zhejiang University, Hangzhou, 310058, China

[§]School of Biomedical Engineering, Shanghai Jiao Tong University, Shanghai 200240, China

[∥]Department of Instrument Science and Engineering, The School of Electronic Information and Electrical Engineering, Shanghai Jiao Tong University, Shanghai 200240, China

[⊥]Pilot Gene Technologies, Hangzhou, 311203, China

[#]College of Life Sciences, University of the Chinese Academy of Sciences, Beijing, 10049, China

[⊗]Savaid Medical School, University of the Chinese Academy of Sciences, Beijing, 10049, China

Supporting Information

ABSTRACT: Digital PCR is a powerful method for absolute nucleic acid quantification with unprecedented accuracy and precision. To promote the wider use and application of digital PCR, several major challenges still exist, including reduction of cost, integration of the instrumental platform, and simplification of operations. This paper describes a reusable microfluidic device that generates nanoliter droplet arrays based on step emulsification for the on-chip multiplex digital PCR of eight samples simultaneously. The device contains two glass plates that can be quickly assembled with prefilled mineral oil. Droplets are simply generated through the arrays of step emulsification nozzles driven by a single pressure controller and are self-assembled into monolayer droplet arrays in U-shaped chambers. The use of mineral oil eliminates bubble generation; thus, no overpressure is required during thermocycling. Moreover, the device can be reused many times after disassembly and a brief cleaning procedure, which significantly reduces the cost of the device per dPCR assays. The device was able to detect template DNA at concentrations as low as 10 copies/μL with a dynamic range of approximately 4 logs. We applied this device in the quantitative assessment of *HER2* copy number variation, which is important for targeted therapy and prognosis of breast cancer. The performance was validated by 16 clinical samples, obtaining similar results to commercial digital PCR. We envision that this low-cost, reusable, and user-friendly device can be broadly used in various applications.

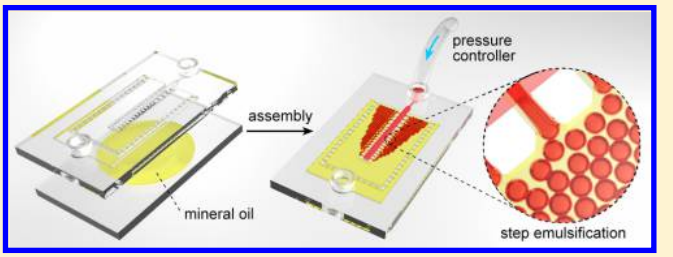

Digital polymerase chain reaction (dPCR), regarded as the "third generation" of PCR technology, is a cutting-edge nucleic acid detection method that achieves absolute quantification of target templates without calibration.[1] In dPCR, samples containing target nucleic acids are divided into tens of thousands of partitions, and each partition contains a few or no copies of target templates. After amplification, the partitions are classified into "positive" or "negative" according to fluorescence intensity, and the original concentrations of the templates can be calculated based on the Poisson algorithm.[1] Compared with conventional real-time quantitative PCR (qPCR), dPCR provides many advantages including high accuracy and sensitivity, the absolute quantification of target nucleic acid without calibration curves,[2,3] and the ability to detect target nucleic acids at low concentration.[4,5] With its outstanding performance, dPCR has been widely used in nucleic acid tests, including gene copy number variation (CNV) analysis,[6] single-cell gene expression analysis,[7] genetic allelic imbalance detection,[8] and noninvasive prenatal testing (NIPT).[9]

The key step in dPCR is the generation of a large number of uniform and separate partitions. There are commonly two strategies: one is chamber-based,[10−13] by which samples are distributed into thousands to tens of thousands of microfabricated chambers; the other is droplet-based,[14−18] by which samples are split into picoliter to nanoliter droplets dispersed in immiscible oil. Although chamber-based methods can achieve equal volume partition with absolute and relocatable positions, they require expensive microfabricated devices and complicated mechanisms to fill the microchambers and avoid cross-contamination. In contrast, droplet-based approaches can

Received: September 21, 2018
Accepted: January 3, 2019
Published: January 4, 2019

DOI: 10.1021/acs.analchem.8b04313
Anal. Chem. XXXX, XXX, XXX−XXX

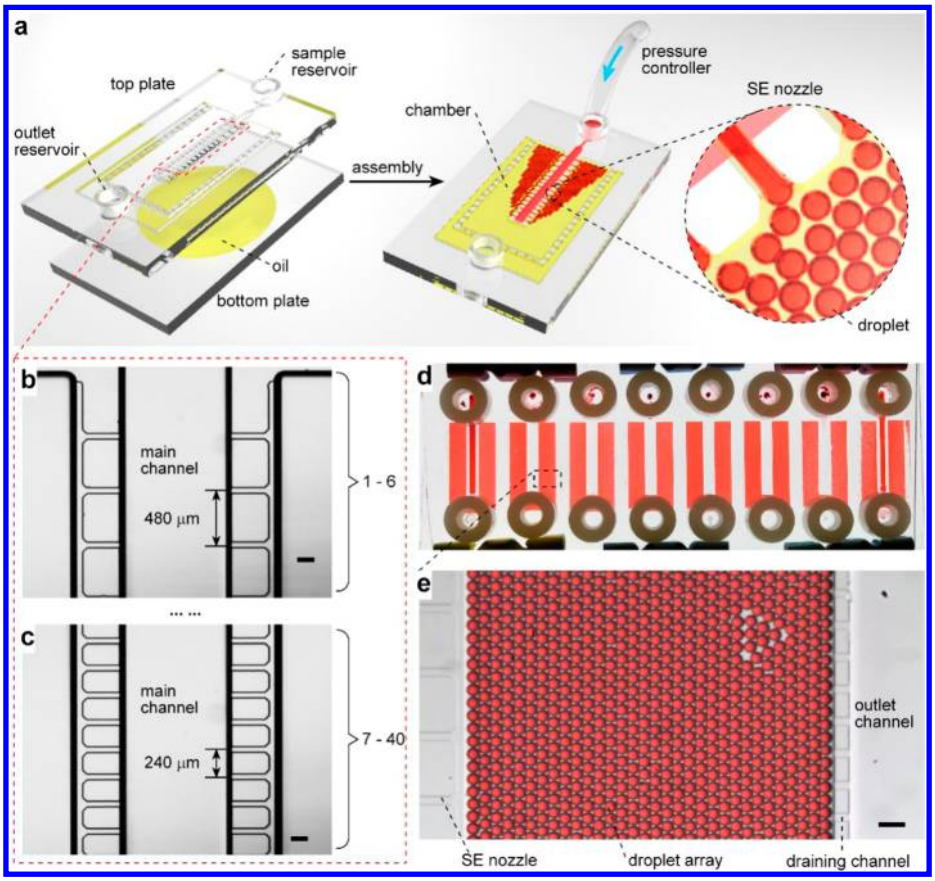

Figure 1. Illustration of the step emulsification (SE) dPCR device. (a) Rapid device assembly and generation of droplets based on SE. Oil was added on the bottom plate and before the top plate was placed onto the bottom plate. After assembly, sample was added to the sample reservoir and pressure was applied via a Tygon tube for droplet generation. (b) Bright-field microphotograph of the upper part of the main channel with 480 μm spacing between adjacent SE nozzles. (c) Microphotograph of the middle and lower parts of the main channel with 240 μm spacing between SE nozzles. (d) A picture of the device with red food-dye droplet arrays generated in all eight chambers. (e) Zoomed-in view of the monolayer droplet array in the right side of the chamber. Scale bars = 200 μm.

incorporate large numbers of droplets in a single device with high throughput, low cost, and simple operation processes.

Droplet-based dPCR relies on microfluidic methods that split samples into monodisperse droplets. The most commonly used methods for droplet generation are T-junctions[19,20] and flow focusing,[19,21] both of which need precise control of flow rates of the dispersed phase and continuous phase, and the volume of droplets is variable depending on flow rates. Recently, several simple methods for droplet generation have been reported which does not rely on microfabricated devices, such as cross-interface emulsification,[22] centrifugal microchannel array droplet generation,[23] particle-templated emulsification,[24] and spinning micropipet liquid emulsification.[25] However, the efficiency, reliability, and system-level integration of these newly developed methods still requires further studies. In the past few years, step emulsification (SE) has emerged as an alternative method for droplet generation with deterministic droplet volume.[26,27] In SE, one liquid flows through a shallow channel and breaks into droplets at the step because of the sudden change in interfacial tension. Compared to the T-junction and flow focusing, SE only needs to control the flow of the dispersed phase and the droplet volume is simply determined by geometric design.[28−32] Consequently, robust and uniform droplets can be obtained through the SE method.

To design an SE dPCR system, parallel SE nozzles followed by a droplet receiving chamber for on-chip droplet array dPCR is preferred because it allows a dramatic increase in droplet generation throughput[33] as well as the integration of on-chip thermal cycling and detection. However, due to high DNA melting temperature (up to 95 °C) during PCR thermal cycling, bubble formation usually occurs in the chamber which inevitably disturbs the droplet array and causes dPCR failures.[13] To overcome this problem, a centrifugal SE chip with a tapered PCR chamber has been developed to guide the assembly of droplet array and the removal of air bubbles generated during thermocycling.[33] Isothermal digital loop-mediated amplification (dLAMP) and digital recombinase polymerase amplification (dRPA) have been realized on SE systems, which bypass the high-temperature obstacle of dPCR.[34,35] Recently, Stilla Technologies introduced a chip that incorporates height variations for generation and transport of monodisperse droplet arrays in rectangular chambers.[36] The suppression of bubble formation is realized by maintaining overpressure during the thermal cycling. However, both systems require microstructures with 3D gradient in height, which are difficult and expensive to fabricate. Moreover, these systems cannot avoid air bubble formation if the delicate 3D structures or overpressure controller are absent. The single use nature of these costly devices makes them not affordable for widespread use. Therefore, to provide low-cost, reliable, and easy-to-use droplet dPCR for research and clinical applications,

DOI: 10.1021/acs.analchem.8b04313
Anal. Chem. XXXX, XXX, XXX−XXX

more efforts toward further reduction of cost and simplification of experimental procedure are required.

This paper describes a reusable microfluidic device that can be easily assembled for SE droplet generation, droplet array self-assembly, PCR amplification, and on-chip dPCR readout. The device is made of two glass plates that can be quickly assembled with microchannels and chambers prefilled with mineral oil. A single pressure controller is used to drive the generation of monolayer arrays of approximately 10 000 droplets for 8 samples in 8 rectangular chambers in 6 min on one device. An array of shallow draining channels around the microchambers is designed to allow the blockage of the droplet array in the chambers and the draining of oil during droplet generation and thermal cycling due to thermal expansion. As mineral oil is used as the continuous phase, on-chip thermal cycling can be performed without applying overpressure to the device. Importantly, the device can be easily reusable by disassembly and removal of DNA and RNA contaminations, dramatically reducing the cost of dPCR assays. The performance of this SE dPCR device is evaluated, and the application in the assessment of human epidermal growth factor receptor 2 (*HER2*) copy number variations (CNV) for clinical samples has comparable results with commercial dPCR platforms.

EXPERIMENTAL SECTION

Fabrication and Operation of the SE dPCR Device. The microfluidic device was fabricated using soda-lime glass plates (Telic, Valencia, CA) patterned by standard photolithography and wet chemical etching techniques.[1] The glass plates were then treated in a plasma cleaner (Harrick Plasma, Ithaca, NY) and silanized by dichlorodimethylsilane (InnoChem Technology Co., Ltd., Beijing, China). The device was assembled, loaded, and used to perform multiplex dPCR as described in Supporting Information.

Application of dPCR for *HER2* CNV Assessment. The dPCR device was applied to assess *HER2* gene CNV in formalin-fixed paraffin-embedded (FFPE) samples provided by Hangzhou Cancer Hospital, Hangzhou, China. The DNA was extracted from FFPE samples and purified using the QIAamp DNA FFPE Tissue Kit (Qiagen, Valencia, CA) according to the manufacturer's protocols. The clinical samples were also detected using our SE dPCR device and QuantStudio 3D Digital PCR System (Thermo Fisher, South San Francisco, CA) to make a comparison.

RESULTS AND DISCUSSION

Design and Operation of the Microfluidic Device. To introduce a reusable dPCR device based on SE, we choose glass as the substrates to make the SE dPCR device. Currently, all SE-based dPCR systems use microfabricated chips that require multidepth microfabrication and permanent bonding of polymeric substrates that cannot be reused. As SE relies on high-precision step microstructures, the deformation of the polymeric substrate during the thermal bonding process needs to be precisely controlled; thus, high cost is expected. In this work, glass substrate is preferred due to its high stability, high flatness, high transparency, and good thermal conductivity. The silanized glass plates can be rapidly assembled and tightly clamped by binder clips. The devices could be disassembled and reused more than 50 times after decontamination, thus greatly reducing the cost of dPCR assays (Figure S5). Further reuse of the device can be realized by resilanization of the device.

The schematic of the SE dPCR device is shown in Figure 1. The main microfabricated feature is a U-shaped chamber (0.75 cm^2 in area) connected to an array of SE nozzles distributed on the two sides of the main channel (Figure 1a). As the main channel is in the middle of the U-shaped chamber, droplets can be formed on both sides of the main channel via SE nozzles. Compared with droplet formation on one side of the main channel, this design reduces the width of the droplet array chamber to 50%, which helps to avoid high static resistance during droplets spreading, and significantly improves the droplet generation efficiency. To further balance the droplet generation rates along the main channel, the spacing between the first 6 SE nozzles from the inlet (480 μm) is designed to be larger than the following SE nozzles (240 μm in spacing) (Figure 1b,c).

To avoid disruption of the droplet array in the chamber, the SE dPCR device must be assembled with prefilled carrier oil without trapping of any air bubble (see details on assembly of the device in Supporting Information and Figure S1). We compared two methods of oil loading: loading through the sample inlets after assembly and directly adding oil to the surface of the bottom plate before assembly. Using the first method, at least eight pipetting steps are required to fill all chambers, and we found that air bubbles trapped in the chamber cannot be fully expelled due to the shallow oil draining channel design (Figure S2a). In contrast, the second method can effectively avoid bubble trapping in the chamber, and only one pipetting step is required (Figure S2b).

To generate the droplet array of samples in the oil-filled chambers by SE, we first loaded samples into the sample reservoirs by an 8-channel pipet. Then, a pressure controller was connected with the sample reservoirs via Tygon tubes to apply pressure and drive the flow of sample from the reservoirs into the main channels (Figure S3), finally reaching at the SE nozzles. When the aqueous solution flowed through the SE nozzles, it was broken down into droplets at the step because of the sudden change of the interfacial tension. Accompanied with droplet arrangement in the droplet array chamber, oil was exhausted to the outlet channels through the oil draining channel (Figure 1d,e), and eventually flowed into the outlet reservoirs. Droplets were generated in the eight independent chambers simultaneously and self-assembled into monolayer droplet arrays in the chambers, each containing 9 000 to 10 000 droplets. Using the optimized design, a uniform droplet size of 84 μm (0.31 nL in volume) and a coefficient of variation (CV) of 2.49% were obtained (Figure S4). More details on optimization of the device design for droplet generation and self-assembly are available in the Supporting Information.

To perform dPCR amplification and detection, the binder clips on both sides of the device were removed and the device was placed on an *in situ* PCR machine for thermal cycling and later imaged on a fluorescence microscope. This droplet generation method only needs a single pressure controller, which is much simpler compared with flow focusing. In addition, mineral oil exhibits excellent thermal stability, which ensures no bubble emergence during thermal cycling.

Quantitative Measurement of *HER2* Gene by dPCR. *HER2* gene is involved in signal transduction for cell growth and differentiation. Approximately 15−30% of breast cancer patients display *HER2* overexpression, which shows a poor

DOI: 10.1021/acs.analchem.8b04313
Anal. Chem. XXXX, XXX, XXX−XXX

prognosis and is likely to metastasize.[37,38] Accordingly, the *HER2* gene serves as an important biomarker for aggressive cancers and a predictor of therapeutic effect in clinical treatment.[37,38] In *HER2* positive cases, treatment with the specific drug Herceptin improves the patients' survival rate and life quality.[39,40] Therefore, accurate assessment of *HER2* copy number is essential for targeted therapy and prognosis.

To demonstrate the quantitative measurement of *HER2* by our SE dPCR device, the *HER2* DNA standard was diluted from 2000 to 10 copies/μL to be used as templates in dPCR experiments. Six premixed PCR reactions, including the negative control, were loaded into the device and generated into droplets in different chambers. During the amplification program, neither droplet fusion nor bubbles was observed, and no overpressure was required. Representative fluorescence microphotographs after amplification cycling are shown in Figure 2a. The droplets containing template DNA showed

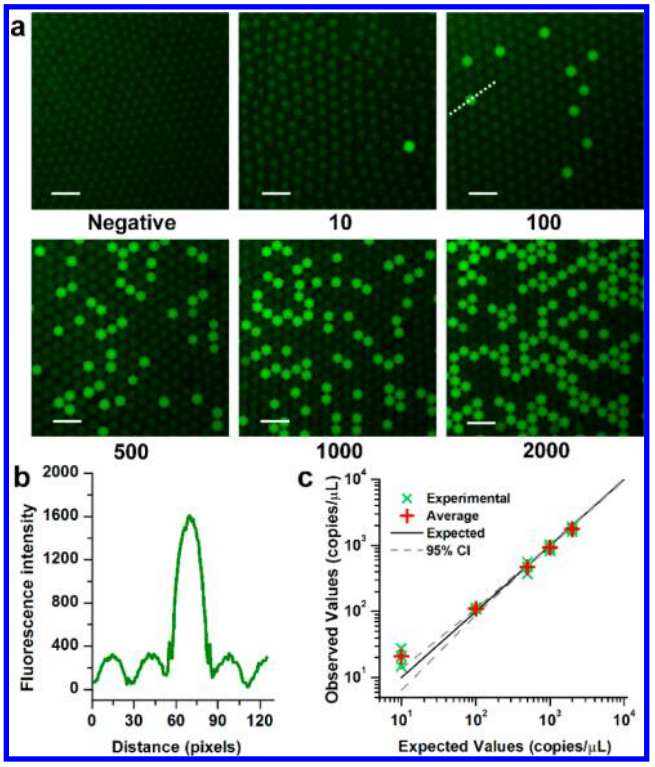

Figure 2. dPCR results on the SE device with different concentrations of *HER2* molecules. (a) Fluorescent microphotographs of droplet array after dPCR with a serial dilution of target DNA templates ranging from 2000 copies/μL to 10 copies/μL and a negative control. (b) A line scan across the microphotograph of the sample with 100 copies/μL templates in panel A shows that fluorescence intensity of positive droplets were more than 4-fold higher than that of negative droplets. (c) The linear correlation between the expected value and the observed copy numbers (black curve) and 95% confidence interval (gray curves). Three experiments were performed at each concentration, with green crosses representing for each experiment and red crosses for the average of the results.

significantly higher fluorescence intensity than the negative droplets (Figure 2b), and the fraction of positive droplets increased proportionally with the concentration of template DNA. As the negative control sample without template DNA showed no false positive results in three experiments using the reused device, this proves that DNA contamination can be eliminated by our device reuse protocol. The linear correlation between the expected value and the observed copy numbers was obtained (R^2 = 0.9951, Figure 2c). The results showed that the calculated template concentration agreed well with the theoretically predicted statistical distribution at each concentration and had a good linear correlation with the expected amounts of templates. The SE device was able to detect template DNA at concentrations as low as 10 copies/μL, with a theoretical dynamic range of approximately 4 logs. According to the Poisson distribution, when the fraction of negative droplets reaches at 20.3%, the detection accuracy is at a maximum. So the most optimized concentration of template DNA is ~500 copies/μL.

***HER2* CNV Assessment in Clinical Samples.** To assess *HER2* CNV status for breast cancer, a duplexed TaqMan PCR assay was introduced for the detection of *HER2* and *RNase P* (a reference gene in CEP14) simultaneously. Purified DNA samples of breast tumors were used to evaluate the performance of our SE dPCR device and Life Technologies QuantStudio 3D dPCR platform. As shown in Figure 3a, the merged microphotograph of FAM and VIC fluorescence channels shows that droplets can be distinguished as *HER2* positive (green), *RNase P* positive (orange), and negative (dark), respectively. The box plots of fluorescence intensity in the FAM and VIC channels also shows that positive and negative droplets can be perfectly distinguished (Figure 3b,c). After enumeration of positive and negative droplets using microphotographs in the two fluorescence channels separately, the concentrations of *HER2* and *RNase P* genes were calculated based on Poisson distribution separately, and *HER2* CNV statuses were obtained for all 16 clinical samples. *HER2* gene is considered as overexpressed if the *HER2*/*RNase P* ratio surpasses 1.5 and normal if the ratio is inferior to 1.2. When the ratio ranges between 1.2 and 1.5, the *HER2* status is considered as in the gray area, in which a second sample collection is required. We calculated the ratio of *HER2* gene and *RNase P* and found that 6 of the samples were *HER2* negative and 10 were *HER2* positive, and the values were with the results carried out with QuantStudio 3D dPCR (Figure 3d,e and Table S1 and Figure S6).

CONCLUSIONS

In this work, we presented a reusable assembled SE device for low-cost and high-throughput digital droplet PCR. The device integrates droplet generation, droplets array self-assembly, droplet dPCR and fluorescence image acquisition for 8 samples on a single device. The device was applied to assess *HER2* CNV status in breast cancer with comparable results as existing commercial platforms. Unlike previous dPCR devices which are designed to be disposable, our device is composed of two glass plates that can be quickly assembled without alignment and can be reused for 50 times after disassembly and a brief decontamination procedure (see Supporting Information and Figure S5 for details). This significantly reduces the cost of the device per dPCR assays. The device does not require the prefilling of oil and thus can be stored dry for a long time, without concern about device expiration due to the preloaded oil. The assembly step with oil dropped on the bottom plate allows the complete filling of microchambers and channels without trapping of air bubbles. Moreover, the use of low-cost mineral oil with a high boiling point effectively avoids the formation of bubbles in droplet array chambers during thermal cycling; thus, no overpressure control over the device is required, and a common *in situ* thermal cycler can be used.

DOI: 10.1021/acs.analchem.8b04313
Anal. Chem. XXXX, XXX, XXX−XXX

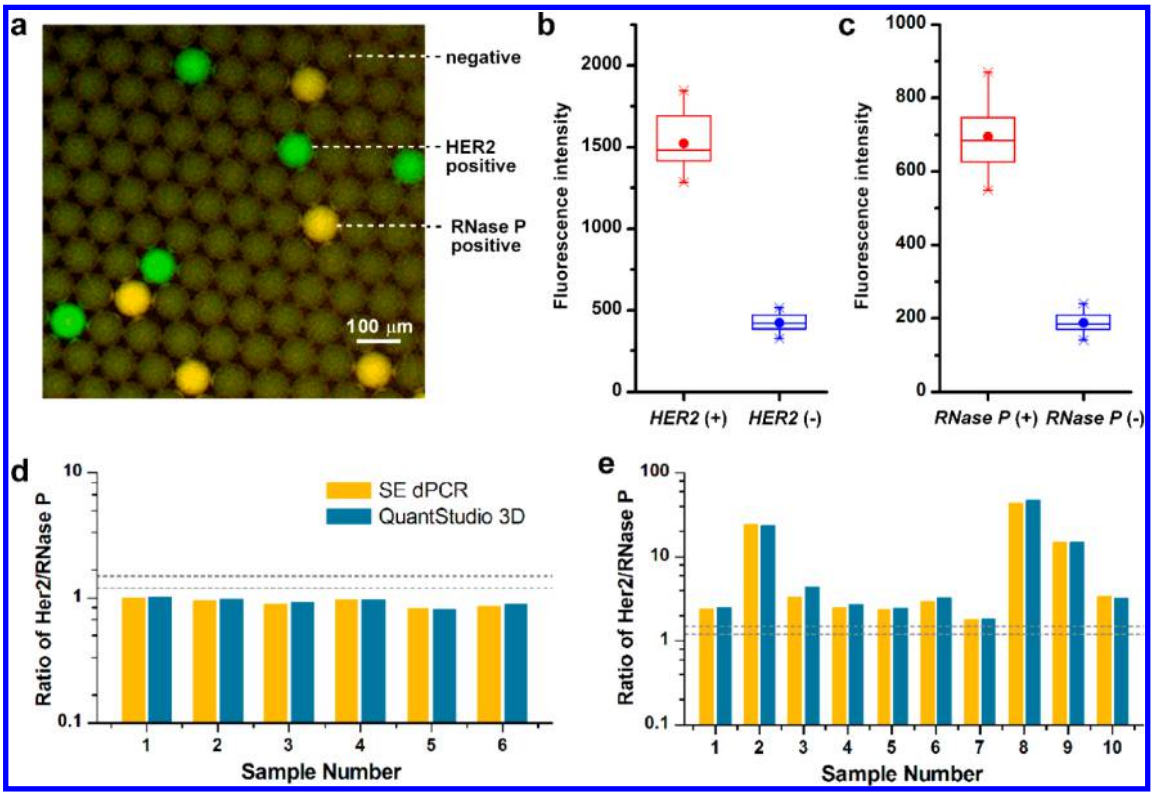

Figure 3. Duplexed TaqMan dPCR for the assessment of the *HER2* gene CNV of breast cancer. (a) A typical fluorescence microphotograph combining the FAM and VIC channels. *HER2* (FAM-labeled) and *RNase P* (VIC-labeled) can be simultaneously detected by SE dPCR. (b) Box plots of fluorescence intensity in the FAM channel for *HER2* positive and negative droplets. (c) Box plots of fluorescence intensity in the VIC channel for *RNase P* positive and negative droplets. (d,e) Detection results of *HER2* copy number variation for (d) *HER2* negative and (e) *HER2* positive clinical samples. The dashed line in panels d and e are threshold levels for overexpression (>1.5) and normal (<1.2).

This feature is especially important as it may allow real-time fluorescence imaging of the droplet array during amplification from above and will set the basis for the development of a fully automated SE dPCR system that integrates sample loading, droplet array generation, thermal cycling, and multichannel fluorescence imaging. We envision that this SE dPCR device can be widely used in research and clinical applications including liquid biopsy, copy number variation, gene expression, and miRNA analysis.

■ ASSOCIATED CONTENT

Supporting Information

The Supporting Information is available free of charge on the ACS Publications website at DOI: 10.1021/acs.analchem.8b04313.

Experimental details, optimization of the device, design for droplet generation and self-assembly, and supporting figures (PDF)

■ AUTHOR INFORMATION

Corresponding Authors

*E-mail: lanying@im.ac.cn.
*E-mail: kelvonpan@zju.edu.cn.
*E-mail: wenbin@im.ac.cn.

ORCID

Feng Shen: 0000-0002-4709-330X
Wenbin Du: 0000-0002-7401-1410

Notes

The authors declare no competing financial interest.

■ ACKNOWLEDGMENTS

This work was supported by the National Key Research and Development Program of China (Grants 2016YFE0205800 and 2016YFC0100900), National Natural Science Foundation of China (Grants 31470221 and 21822408), Beijing Municipal Science & Technology Commission (No. Z161100000116042), Key Research Program of the Chinese Academy of Sciences (Grant KFZD-SW-219-4), National Science and Technology Major Special Project of Transgenes (Grant 2018ZX08022001), and Open Research Fund of State Key Laboratory of Bioelectronics, Southeast University.

■ REFERENCES

(1) Kreutz, J. E.; Munson, T.; Huynh, T.; Shen, F.; Du, W.; Ismagilov, R. F. *Anal. Chem.* **2011**, *83*, 8158−8168.

(2) Pinheiro, L. B.; Coleman, V. A.; Hindson, C. M.; Herrmann, J.; Hindson, B. J.; Bhat, S.; Emslie, K. R. *Anal. Chem.* **2012**, *84*, 1003−1011.

(3) Hindson, B. J.; Ness, K. D.; Masquelier, D. A.; Belgrader, P.; Heredia, N. J.; Makarewicz, A. J.; Bright, I. J.; Lucero, M. Y.; Hiddessen, A. L.; Legler, T. C.; Kitano, T. K.; Hodel, M. R.; Petersen, J. F.; Wyatt, P. W.; Steenblock, E. R.; Shah, P. H.; Bousse, L. J.; Troup, C. B.; Mellen, J. C.; Wittmann, D. K.; Erndt, N. G.; Cauley, T. H.; Koehler, R. T.; So, A. P.; Dube, S.; Rose, K. A.; Montesclaros, L.; Wang, S.; Stumbo, D. P.; Hodges, S. P.; Romine, S.; Milanovich, F. P.; White, H. E.; Regan, J. F.; Karlin-Neumann, G. A.; Hindson, C. M.; Saxonov, S.; Colston, B. W. *Anal. Chem.* **2011**, *83*, 8604−8610.

(4) Sanders, R.; Huggett, J. F.; Bushell, C. A.; Cowen, S.; Scott, D. J.; Foy, C. A. *Anal. Chem.* **2011**, *83*, 6474−6484.

(5) Whale, A. S.; Huggett, J. F.; Cowen, S.; Speirs, V.; Shaw, J.; Ellison, S.; Foy, C. A.; Scott, D. *J. Nucleic Acids Res.* **2012**, *40*, No. e82.

DOI: 10.1021/acs.analchem.8b04313
Anal. Chem. XXXX, XXX, XXX−XXX

(6) Qin, J.; Jones, R. C.; Ramakrishnan, R. *Nucleic Acids Res.* **2008**, *36*, No. e116.
(7) White, A. K.; Heyries, K. A.; Doolin, C.; Vaninsberghe, M.; Hansen, C. L. *Anal. Chem.* **2013**, *85*, 7182−7190.
(8) Fan, H. C.; Quake, S. R. *Anal. Chem.* **2007**, *79*, 7576−7579.
(9) Lo, Y. M.; Lun, F. M.; Chan, K. C.; Tsui, N. B.; Chong, K. C.; Lau, T. K.; Leung, T. Y.; Zee, B. C.; Cantor, C. R.; Chiu, R. W. *Proc. Natl. Acad. Sci. U. S. A.* **2007**, *104*, 13116−13121.
(10) Men, Y.; Fu, Y.; Chen, Z.; Sims, P. A.; Greenleaf, W. J.; Huang, Y. *Anal. Chem.* **2012**, *84*, 4262−4266.
(11) Heyries, K. A.; Tropini, C.; Vaninsberghe, M.; Doolin, C.; Petriv, O. I.; Singhal, A.; Leung, K.; Hughesman, C. B.; Hansen, C. L. *Nat. Methods* **2011**, *8*, 649−651.
(12) Shen, F.; Du, W.; Kreutz, J. E.; Fok, A.; Ismagilov, R. F. *Lab Chip* **2010**, *10*, 2666−2672.
(13) Gou, T.; Hu, J.; Wu, W.; Ding, X.; Zhou, S.; Fang, W.; Mu, Y. *Biosens. Bioelectron.* **2018**, *120*, 144−152.
(14) Hatch, A. C.; Fisher, J. S.; Tovar, A. R.; Hsieh, A. T.; Lin, R.; Pentoney, S. L.; Yang, D. L.; Lee, A. P. *Lab Chip* **2011**, *11*, 3838−3845.
(15) Kiss, M. M.; Ortoleva-Donnelly, L.; Beer, N. R.; Warner, J.; Bailey, C. G.; Colston, B. W.; Rothberg, J. M.; Link, D. R.; Leamon, J. H. *Anal. Chem.* **2008**, *80*, 8975−8981.
(16) Kumaresan, P.; Yang, C. J.; Cronier, S. A.; Blazej, R. G.; Mathies, R. A. *Anal. Chem.* **2008**, *80*, 3522−3529.
(17) Xu, X.; Yuan, H.; Song, R.; Yu, M.; Chung, H. Y.; Hou, Y.; Shang, Y.; Zhou, H.; Yao, S. *Biomicrofluidics* **2018**, *12*, No. 014103.
(18) Tsukuda, M.; Wiederkehr, R. S.; Cai, Q.; Majeed, B.; Fiorini, P.; Stakenborg, T.; Matsuno, T. *Jpn. J. Appl. Phys.* **2016**, *55*, No. 04EM05.
(19) Seemann, R.; Brinkmann, M.; Pfohl, T.; Herminghaus, S. *Rep. Prog. Phys.* **2012**, *75*, 016601.
(20) Xu, J. H.; Li, S. W.; Tan, J.; Luo, G. S. *Microfluid. Nanofluid.* **2008**, *5*, 711−717.
(21) Anna, S. L.; Bontoux, N.; Stone, H. A. *Appl. Phys. Lett.* **2003**, *82*, 364−366.
(22) Xu, P.; Zheng, X.; Tao, Y.; Du, W. *Anal. Chem.* **2016**, *88*, 3171−7.
(23) Chen, Z.; Liao, P.; Zhang, F.; Jiang, M.; Zhu, Y.; Huang, Y. *Lab Chip* **2017**, *17*, 235−240.
(24) Hatori, M. N.; Kim, S. C.; Abate, A. R. *Anal. Chem.* **2018**, *90*, 9813−9820.
(25) Chen, Z.; Fu, Y.; Zhang, F.; Liu, L.; Zhang, N.; Zhou, D.; Yang, J.; Pang, Y.; Huang, Y. *Lab Chip* **2016**, *16*, 4512−4516.
(26) Sugiura, S.; Nakajima, M.; Iwamoto, S.; Seki, M. *Langmuir* **2001**, *17*, 5562−5566.
(27) Sugiura, S.; Nakajima, M.; Oda, T.; Satake, M.; Seki, M. *J. Colloid Interface Sci.* **2004**, *269*, 178−185.
(28) Dangla, R.; Fradet, E.; Lopez, Y.; Baroud, C. N. *J. Phys. D: Appl. Phys.* **2013**, *46* (11), 114003.
(29) Dangla, R.; Kayi, S. C.; Baroud, C. N. *Proc. Natl. Acad. Sci. U. S. A.* **2013**, *110*, 853−858.
(30) Sugiura, S.; Nakajima, M.; Seki, M. *Langmuir* **2002**, *18*, 5708−5712.
(31) Sugiura, S.; Nakajima, M.; Seki, M. *Langmuir* **2002**, *18*, 3854−3859.
(32) Ofner, A.; Moore, D. G.; Rühs, P. A.; Schwendimann, P.; Eggersdorfer, M.; Amstad, E.; Weitz, D. A.; Studart, A. R. *Macromol. Chem. Phys.* **2017**, *218*, 1600472.
(33) Schuler, F.; Trotter, M.; Geltman, M.; Schwemmer, F.; Wadle, S.; Dominguez-Garrido, E.; Lopez, M.; Cervera-Acedo, C.; Santibanez, P.; von Stetten, F.; Zengerle, R.; Paust, N. *Lab Chip* **2016**, *16*, 208−216.
(34) Schuler, F.; Schwemmer, F.; Trotter, M.; Wadle, S.; Zengerle, R.; von Stetten, F.; Paust, N. *Lab Chip* **2015**, *15*, 2759−2766.
(35) Schuler, F.; Siber, C.; Hin, S.; Wadle, S.; Paust, N.; Zengerle, R.; von Stetten, F. *Anal. Methods* **2016**, *8*, 2750−2755.
(36) Madic, J.; Zocevic, A.; Senlis, V.; Fradet, E.; Andre, B.; Muller, S.; Dangla, R.; Droniou, M. E. *Biomol. Detect. Quantif.* **2016**, *10*, 34−46.
(37) Baselga, J.; Gianni, L.; Geyer, C.; Perez, E. A.; Riva, A.; Jackisch, C. *Semin. Oncol.* **2004**, *31*, 51−57.
(38) Bossard, C.; Bieche, I.; Le Doussal, V.; Lidereau, R.; Sabourin, J. C. *Anticancer Res.* **2005**, *25*, 4679−4683.
(39) Slamon, D. J.; Leyland-Jones, B.; Shak, S.; Fuchs, H.; Paton, V.; Bajamonde, A.; Fleming, T.; Eiermann, W.; Wolter, J.; Pegram, M.; Baselga, J.; Norton, L. *N. Engl. J. Med.* **2001**, *344*, 783−792.
(40) Lee, S.; Yang, W.; Lan, K. H.; Sellappan, S.; Klos, K.; Hortobagyi, G.; Hung, M. C.; Yu, D. *Cancer Res.* **2002**, *20*, 5703−5710.

DOI: 10.1021/acs.analchem.8b04313
Anal. Chem. XXXX, XXX, XXX−XXX

DOI: 10.1021/acs.analchem.8b04313

Supporting Information for

Assembled Step Emulsification Device for Multiplex Droplet Digital PCR

Mengyue Nie[1, 6], Meng Zheng[1, 7], Caiming Li[1, 6], Feng Shen[3], Manhua Liu[4], Haibei Luo[5], Xiaohui Song[5], Ying Lan[1]*, Jian-Zhang Pan[2]*, Wenbin Du[1, 6, 7]*

[1] State Key Laboratory of Microbial Resources, Institute of Microbiology, Chinese Academy of Sciences, 100101, Beijing, China.

[2] Institute of Microanalytical Systems, Department of Chemistry, Zhejiang University, Hangzhou, 310058, China

[3] School of Biomedical Engineering, Shanghai Jiao Tong University, Shanghai 200240, China

[4] Department of Instrument Science and Engineering, The School of Electronic Information and Electrical Engineering, Shanghai Jiao Tong University, Shanghai 200240, China

[5] Pilot gene Technologies, Hangzhou, 311203, China

[6] College of Life Sciences, University of the Chinese Academy of Sciences, Beijing, 10049, China

[7] Savaid Medical School, University of the Chinese Academy of Sciences, Beijing, 10049, China

* Corresponding authors: Ying Lan, lanying@im.ac.cn; Jian-Zhang Pan, kelvonpan@zju.edu.cn; Wenbin Du, wenbin@im.ac.cn.

Contains

Number of pages:10

Number of figures:6

Number of tables:1

Supplemental Materials and Methods

1. Fabrication of the microfluidic device

The microfluidic device was fabricated using soda-lime glass plates (Telic, Valencia, CA, USA) patterned by standard photolithography and wet chemical etching techniques[1]. The photomasks were designed using AutoCAD (San Rafael, CA, USA) and ordered from MicroCAD (Shenzhen, China). The top plate was fabricated by a two-step HF etching process[2]. The chambers, main channels and oil channels were etched 90 μm in depth, while the SE nozzles (300 μm in length, 60 μm in width) and oil draining channels (100 μm in length, 60 μm in width) surrounding the chambers were etched 20 μm in depth. There is a 50 μm step between the nozzles and the chamber as they are different in height. Two access holes on the top plate were drilled by a 0.8 mm diamond drill bit, and two reservoirs were stuck to the glass plate over the drilled holes by epoxy. The bottom plate was a plain glass plate without microfabricated structures. The glass plates were thoroughly cleaned with deionized water and ethanol and dried with nitrogen gas. Then, the glass plates were treated in a plasma cleaner (Harrick Plasma, Ithaca, NY, USA) and silanized by dichlorodimethylsilane (InnoChem Technology Co., Ltd., Beijing, China).

2. Device assembly and sample loading

The microfluidic device was preloaded with an emulsion oil containing surfactants before being assembled. As illustrated in Fig. S1, oil was dropped on the surface of the bottom plate by a dropper, and then the top plate was laid on top of the bottom plate with the micropatterns facing down, such that the entire microfluidic patterns and gap of the two glass plates were filled with oil. The two plates were assembled and tightly clamped by binder clips. The oil recipe we used was a mixture of light mineral oil (Sigma-Aldrich, St. Louis, MO, USA) and *n*-tetradecane (TCI, Beijing, China) at a ratio of 1:1 (w/w), combined with stabilizing surfactants including 3% w/w Abil EM90 (Evonik Industries, Essen, Germany) as described previously[3]. A volume of 10 μL of the reaction mixture was loaded into each of the 8 sample reservoirs by an 8-channel pipette. A pressure controller (MesoBioSystem, Wuhan, China) was then connected to the sample reservoirs by Tygon tubes which can be tightly plugged into the top of the reservoirs. We applied 30 mbar air pressure using the pressure controller to drive droplet generation. In each chamber, approximately 10,000 droplets can be generated in 6 min and self-assembled as a monolayer droplet array. Afterward, the clips were unclamped, and the device was placed on TC1 Thermal Cycler (Pilot Gene Technologies, Hangzhou, China) for PCR reaction. To reuse the device, the glass plates could be disassembled and washed by water with dishwashing

detergent, followed by immersion in DNA-ExitusPlus™ (AppliChem GmbH, Darmstadt, Germany) for 5 minutes to remove DNA contaminations. The plates were then cleaned in an ultrasonic bath with ethanol, blow dried with nitrogen gas, and kept in clean Petri dishes for the next use.

3. Droplet dPCR

Different concentrations of *HER2* (*ERbb2*) DNA standards and several extracted DNA solutions from clinical samples were used as the target DNA to test the performance of our SE dPCR device. All reaction components were premixed off-chip before making the droplets. The *HER2* DNA standard is a commercially reagent from NIST of USA, and the copy number is given in the reagent instructions which were certified by qPCR and dPCR assays. The *HER2* DNA stock solution (Standard Reference Material® 2373, NIST, USA) was serially diluted, and the final template concentrations in the PCR mixture ranged from 10 copies/μL to 2000 copies/μL. The reaction mix (15 μL) was prepared in 0.2 mL tubes, consisting of 7.5 μL of PCR mixture, 1.5 μL of primers and probes, 4 μL of double distilled water and 2 μL of template DNA. Negative control reactions were performed using sterile double-distilled water instead of template DNA in the reaction mix to detect the presence of contamination. For digital quantification of CNV of breast cancer, *HER2* gene was amplified using forward primer 5'-GGGCTCTTTGCAGGTCTCTCC-3', reverse primer 5'-CAGCAAGAGTCCCCATCCTAG-3' and probe 5'-FAM-AGCAAACCCCTATGTCCACAAGGGGCT-bhq1-3', and *Rnase P* gene was amplified using forward primer 5'-GCGGAGGGAAGCTCATCAGTG-3', reverse primer 5' CCCTAGTCTCAGACCTTCCCAA-3' and probe 5'-VIC-ACATGGGAGTGGAGTGACAGG-bhq1-3'.

The PCR mix with a volume of 10 μL was then pipetted into each sample reservoir to form droplets on the device by SE to carry out the dPCR experiment. The PCR amplification protocol included 10 min activation of the Taq polymerase at 95 °C, followed by 40 cycles of 15 s denaturation at 95 °C and 60 s annealing at 60 °C. The experiments were carried out three times to test the repeatability of the method.

4. Clinical sample detection

The dPCR system was applied to assess *HER2* gene CNV in 16 formalin-fixed paraffin-embedded (FFPE) samples kindly provided by Hangzhou Cancer Hospital, Hangzhou, China. Histological examinations confirmed that each section contained at least 30% tumor cells, and all of the FFPE samples had previously been assessed for HER2 status with FISH (PathVysion HER-2 DNA probe kit, Abbott, USA). According to

the FISH data, 10 of the samples were identified as positive for HER2, and 6 were identified as negative. The DNA was extracted from FFPE samples and purified using the QIAamp DNA FFPE Tissue Kit (Qiagen, Valencia, CA, USA) according to the manufacturer's protocols. The extracted DNA concentrations were measured with a NanoDrop ND-1000 spectrophotometer (Thermo Fisher Scientific, South San Francisco, CA, USA).

In parallel to the test on our SE dPCR device, the clinical samples were also detected using QuantStudio™ 3D Digital PCR System (Thermo Fisher Scientific, South San Francisco, CA, USA) to make a comparison. The final 15 μL of the TaqMan PCR reaction mixture was made up of 7.5 μL of 2× QuantStudio™ 3D Digital PCR Master Mix, 1.5 μL of 10× primer/probe mix (at a final concentration of 900 nM for each primers and 250 nM for each probes), and 6 μL of diluted FFPE DNA. The PCR mix was then loaded into the QuantStudio™ 3D Digital PCR Chip, which has 20000 mini-chambers. We used the ProFlex™ 2× Flat PCR System to carry out the digital PCR, and the thermal cycling profile included 10 min incubation at 96 °C, followed by 39 cycles of 30 s at 96 °C and 1 min at 60 °C. The chip was read using the QuantStudio™ 3D Digital PCR instrument, and the subsequent analysis was performed with the QuantStudio 3D Analysis Suite Software.

5. Data acquisition and analysis

After dPCR amplification, fluorescence imaging was performed by a CoolSNAP HQ^2 charge-coupled device camera (Photometrics, Tucson, AZ) mounted to an inverted fluorescence microscope (Eclipse Ti-E, Nikon, Tokyo, Japan). Fluorescence microphotographs were captured on the FAM (excitation: 480/40 nm; emission: 527/30 nm) and VIC (excitation, 535/50 nm; emission, 590 nm longpass) fluorescence channels, and 4X and 10X objectives were used for capturing fluorescence microphotographs of the droplet arrays in the chambers by using the large image scanning function of NIS Elements AR software (Nikon, Tokyo, Japan). Microphotographs were analyzed using the ImageJ software (NIH, Bethesda, MD, USA) to measure the size and fluorescence intensity of droplets.

We counted the total number of droplets in each chamber (about 9,000 ~ 10,000 droplets) and the number of positive droplets. And the concentration of target DNA templates were calculated according to Poisson distribution principle as the following equation:

$$\text{Concentration} = -\frac{\ln(1-\frac{d}{n})}{V} \quad (1)$$

Where n is the total number of droplets in each chamber, d is the number of positive droplets, d/n is the fraction of positive droplets, and V is the droplet volume. Thus, template concentration of each sample is obtained. Further data analysis was done with OriginPro 8 (OriginLab Corporation, Northampton, USA).

Optimization of the device design for droplet generation and self-assembly

To realize continuous droplet generation, as well as the self-assembly of monolayer droplet arrays in the chamber, a key problem we faced was the accumulation of droplets at the outlets of the SE nozzles that confers hydrostatic resistance toward the generation of following droplets. Previously, this problem could be solved by using confinement gradients at the nozzles to propel the droplet away from the nozzles[4], or by transporting the droplets away from the SE nozzles due to density difference and centrifugal force. However, these methods either requires fabrication of the chamber with continuous height variations which is impossible using standard wet etching technique, or limited the device and instrumental setup to centrifugal system.

In our early design in which a uniform nozzle spacing of 240 μm was used, the droplet generation rate was much faster at the nozzle close to the inlet, causing rapid accumulation of droplets at the upper region of the chamber. This outcome affected the self-assembly of the droplet array and resulted in the coalescence of droplets. (Fig. S4a, b). To solve this problem, we introduced a modified design with non-uniform spacing between nozzles. The spacing between the first 6 SE nozzles from the inlet (480 μm) is designed to be larger than the following SE nozzles (240 μm in spacing). The optimized design ensures more uniform droplet generation rates between nozzles and avoids the accumulation of too many droplets on top of the chamber. Consequently, a more uniform monolayer droplet array was obtained (Fig. S4c, d). As shown by the time series microphotographs (Fig. S4e), monolayer droplet array containing ~10,000 droplets which filled the whole chamber, can be obtained in 6 min with very few coalescences. According to our experimental results, the droplet volume is influenced by the width and depth of the channel and the distance between the nozzles and the step, but it doesn't correlated with the channel length. We have tested some design in different channel size and found a configuration that is able to produce droplets suitable for digital PCR. And the flow of the dispersed phase will not influence the droplet size within the tested conditions. The mean droplet diameter was 84 μm, which equates to a mean droplet volume of 0.31 nL, and the coefficient of variation (CV) was as low as 2.49%.

The reusability of the device

We repeated the experiments for 50 times using the same device to test the reusability of the glass chips. We performed the experiments on two chambers of one device: chamber A was used to detect *HER2* DNA with a concentration of 1200 copies/μL in theory, and chamber B was used to detect the negative control. After our decontamination procedure, the second experiment were set up which use chamber B for detecting positive sample, and chamber A for the negative control. The time series detection results of both chambers were shown in Fig. S5. The average number of template DNA was 1132.7 copies/μL with a coefficient of variation (CV) of 8.84% (n=50). And the negative control showed no positive amplification, which indicated that there were no contamination from the previous assays on device during the reuse process.

Consistency analysis of detection results of SE dPCR device and QuantStudio 3D platform

We performed Kappa analysis and correlation analysis to compare the detection consistency of the SE dPCR device and QuantStudio 3D platform. Table 1 showed the detection results of clinical samples carried out by two methods, and Kappa coefficient was calculated according to the following equation:

$$k = (Po - Pe) / (1-Pe) \quad (1)$$

Where $Po = (6+10)/16 = 1$, $Pe = (6*6+10*10)/16^2 = 17/32$, so Kappa coefficient = 1.

The correlation analysis was shown in Fig S6, and the detection results of SE dPCR device had a good linear correlation with the QuantStudio 3D platform (Pearson's r = 0.998).

REFERENCES:

(1) He, Q.; Chen, S.; Su, Y.; Fang, Q.; Chen, H. *Anal. Chim. Acta* **2008**, *628*, 1-8.

(2) Cai, D.; Xiao, M.; Xu, P.; Xu, Y. C.; Du W. *Lab Chip* **2014**, *14*, 3917-3924.

(3) Xu, P.; Zheng, X.; Tao, Y.; Du W. *Anal. Chem.* **2016**, *88*, 3171-3177.

(4) Madic, J.; Zocevic, A.; Senlis, V.; Fradet, E.; Andre, B.; Muller, S.; Dangla, R.; Droniou, M. E. *Biomol. Detect. Quantif.* **2016**, *10*, 34-46.

Table S1 Consistency of SE dPCR and QuantStudio™ 3D (Life Technologies) in assessment of HER2 copy number variation (CNV) in clinical samples.

		SE dPCR		Total
		Positive	Negative	
QuantStudio™ 3D	Positive	6	0	6
	Negative	0	10	10
Total		6	10	16

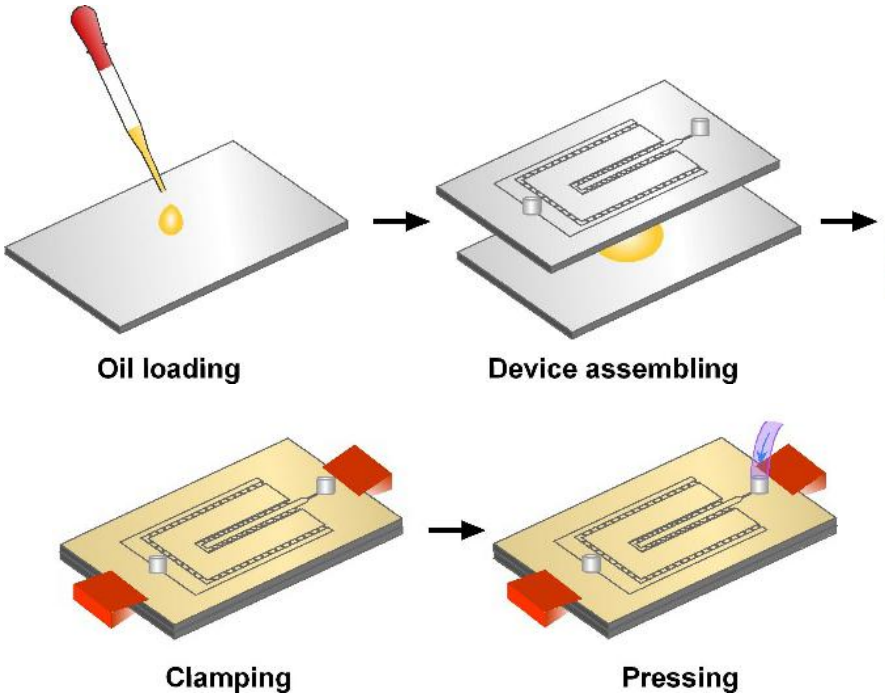

Figure S1 Illustration of the oil loading and device assembling process.

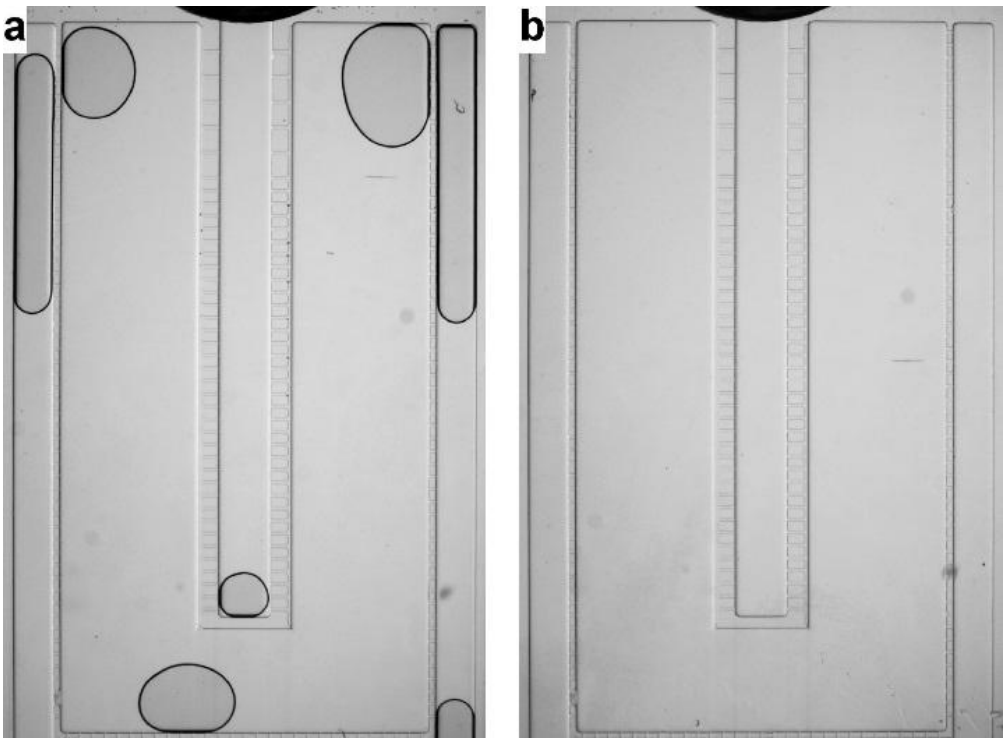

Figure S2 Comparison of the two ways for oil loading. (A) Oil was loaded from the sample reservoir. (B) Oil was loaded on the surface of the bottom glass plate.

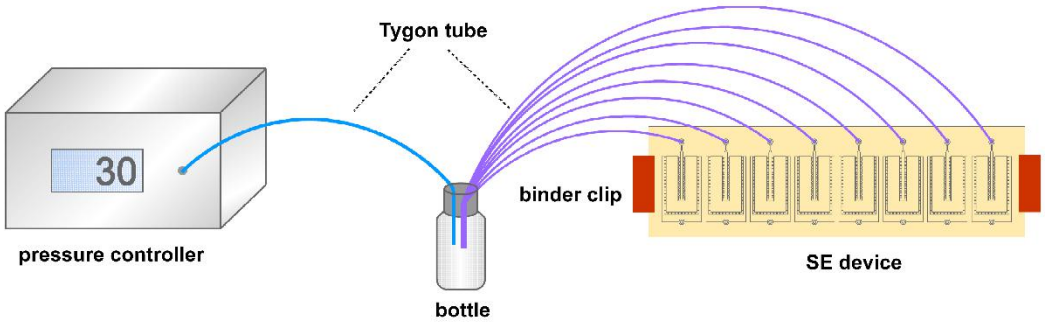

Figure S3 Illustration of the setups for SE droplet generation. The Pressure controller were connected with a pressure buffer bottle. Uniform pressure was distributed to all eight channels of the microfluidic device via eight Tygon tubes.

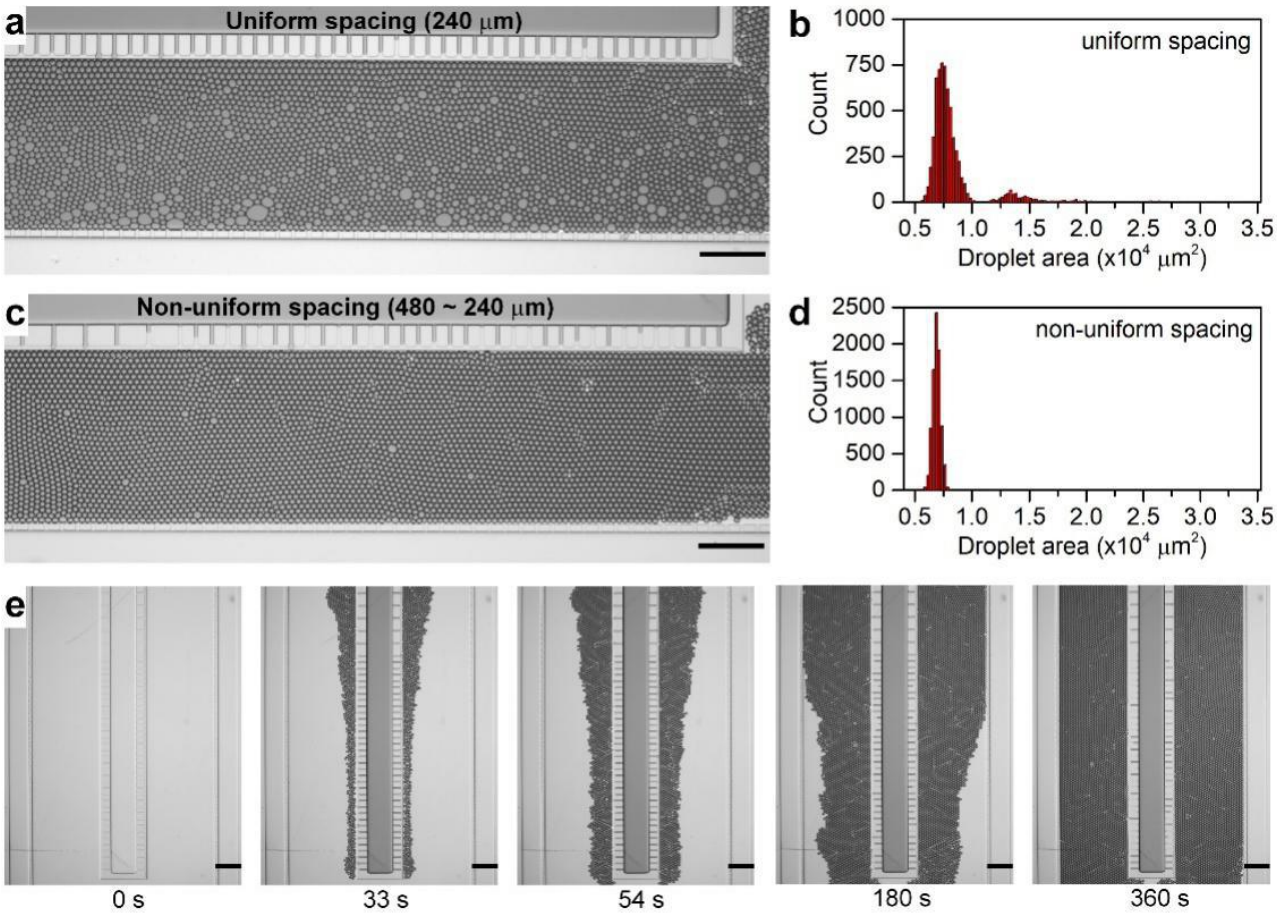

Figure S4 Effect of spacings between SE nozzles on droplet generation. (a, b) Typical microphotograph and area histogram of the droplets generated by device with consistent 240-μm spacing between adjacent SE nozzles. (c, d) Typical microphotograph and area histogram of the droplets generated by device with non-uniform spacing SE nozzles as shown in Fig. 1b-c. (e) Generation of monolayer droplet array in the chamber using nozzle spacing design as shown in Fig. 1b-c. Time series microphotographs were taken at 0 s, 33 s, 54 s, 180 s and 360 s after sample loading. Scale bars=1 mm.

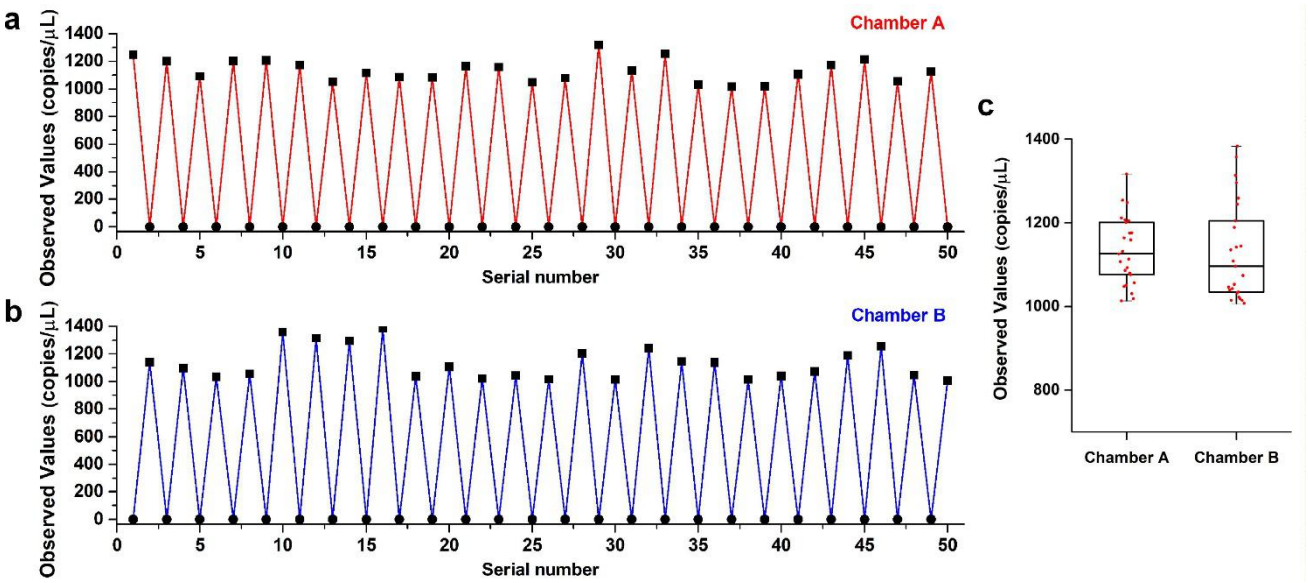

Figure S5 dPCR results of 50 times repeated experiments on two chambers of the same SE device. (a) Statistical illustration of the detection results performed on Chamber A. (b) Statistical illustration of the detection results performed on Chamber B. (c) Box plots for positive results (n=25) performed on Chamber A and Chamber B.

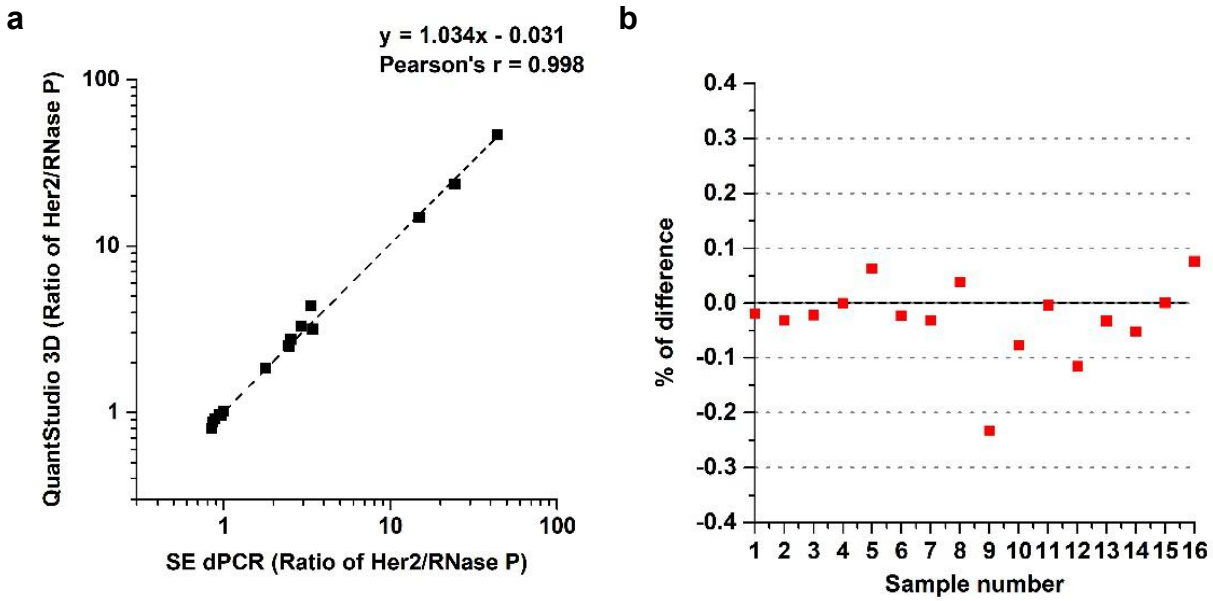

Figure S6 (a) Correlation analysis and (b) percent of difference of clinical sample detection results performed on SE dPCR device and QuantStudio™ 3D platform.